Japanese Journal of Applied Physics
Vol. 44, No. 12, 2005, pp. 8314–8321
10.1143/JJAP.44.8314

New Two-Diode Model for Detailed Analysis of Multicrystalline Silicon Solar Cells

Ken-ichi KUROBE and Hiroyuki MATSUNAMI

Department of Electronic Science and Engineering, Kyoto University, Yoshida-Honmachi, Sakyo, Kyoto 606-8501, Japan

(Received May 9, 2005; accepted August 15, 2005; published December 8, 2005)

In order to extract electrical properties of multicrystalline silicon (Mx-Si) solar cells precisely, current–voltage (I–V) measurement in the dark condition was carried out. A new two-diode model, which includes a diffusion-current dominant area (DCA) and a recombination-current dominant area (RCA), with nonequivalent series resistances, was proposed as a new equivalent circuit. Electrical properties as fitting parameters were successfully extracted using a successive approximation method. This characterization derived J_{01} and J_{02}, which are the diode saturation current densities for $n = 1$ and 2 diodes, respectively. To ensure this diode model, temperature characteristics were measured, and the validity of this model was shown through calculation of the energy band gap from J_{01}. J_{01} and J_{02} indicate a power factor and a loss factor of solar cells, respectively, which are newly proposed to classify solar cell performance. [DOI: 10.1143/JJAP.44.8314]

KEYWORDS: multicrystalline silicon, solar cell, two-diode model, saturation current, power factor, loss factor

1. Introduction

Multicrystalline silicon (Mx-Si) is widely used for solar cells in view of its adequate conversion efficiency (η). However, grain boundaries in Mx-Si solar cells mainly cause the relatively low η compared with those of monocrystalline silicon (c-Si) ones.[1] In order to comprehend the output performance of Mx-Si solar cells, it is important to analyze their electrical properties, such as ideality factor (n), short-circuit current density (J_{SC}), open-circuit voltage (V_{OC}), series resistance (R_s), shunt resistance (R_{sh}),[2] and fill factor (FF), from their current–voltage (I–V) characteristics in the dark or under illumination.

Ordinarily, the electrical properties of solar cells have been analyzed using a simple equivalent circuit.[3–6] However, Mx-Si solar cells depend on many factors such as spatial distribution of lifetime (τ_n for electron) and segregation of lifetime killers,[7] which cause different electrical properties. A new equivalent circuit must be studied for analyzing Mx-Si solar cells, because a simple equivalent circuit cannot include the factors that are inherent to Mx-Si solar cells.

In this paper, a new equivalent circuit model for Mx-Si solar cells is proposed, and I–V characteristics are analyzed using this model in the dark, which is convenient for reliable measurement. To confirm the validity of the electrical properties from this analysis, τ_n and V_{OC} calculated from the measured saturation current density are compared with those obtained by other measurements, such as reverse recovery switching transient analysis and I–V measurement under illumination.

2. Experimental

Five Mx-Si solar cells were used for the characterization. Three of them (cells-A, -B, and -C) were used to confirm the validity of minority-carrier lifetimes from calculation of saturation current densities derived by a fitting method described in §3. The other two (cells-T1 and -T2) were used to confirm this diode model through calculation of the energy band gap (E_g) from the saturation current densities derived by the same method. Detailed experimental conditions and results are shown in ref. 8.

Each cell has a $125 \times 125\,mm^2$ size, a $300\,\mu m$ thickness, a conventional $n^+/p/p^+$ structure, and silicon nitride passivation coating. The bulk resistivity, carrier concentration, and Hall mobility were found as $1–2\,\Omega\cdot cm$, $(1–2) \times 10^{16}\,cm^{-3}$, and $200–300\,cm^2/(V\cdot s)$, respectively, according to Hall effect measurements. The junction depth was about $0.2–0.3\,\mu m$. The photovoltaic characteristics of these cells were previously measured as shown in Table I.

Table I. Photovoltaic characteristics of cells-A, -B, -C, -T1, and -T2 ($100\,mW/cm^2$, AM 1.5).

	η (%)	V_{OC} (V)	J_{SC} (mA/cm^2)	FF
Cell-A	14.4	0.602	32.7	0.732
Cell-B	12.6	0.576	30.9	0.712
Cell-C	11.0	0.567	28.3	0.689
Cell-T1	8.6	0.592	28.5	0.508
Cell-T2	10.1	0.601	31.4	0.535

Dark current density–voltage (J–V) curves of solar cells were measured in the forward and reverse directions using a DC power supply. The maximum current was 6 A, which corresponds to a $3.8 \times 10^{-2}\,A/cm^2$ current density. Between the cell and the DC power supply, a series resistor of $0.1\,\Omega$ was inserted in order to measure the current from the potential difference across the resistor. All contacts were connected with solder to minimize errors due to contact resistance while measuring. Current and voltage were measured with high-input-impedance digital multimeters.

For cells-A, -B, and -C, J–V measurement was carried out at room temperature, while for cells-T1 and -T2, at temperatures from 20 to 100°C in steps of 20°C.

2.1 Simple diode model

Figure 1 shows the J–V curve of cell-A in a semi-log scale. n was obtained as 1.81 from the exponentially increasing region. Theoretical lines are also shown as reference for $n = 1$ and 2 with each arbitrary diode saturation current density (J_0).

Table II shows the electrical properties of cells-A, -B, and -C obtained from individual J–V curves using a simple diode model. Series resistance R_s ($\Omega\cdot cm^2$) was derived from the slope in the region of higher current density in the forward direction. In order to estimate the true series resistance from the forward J–V curve, a linearly increasing region is required. In this measurement, however, the maximum

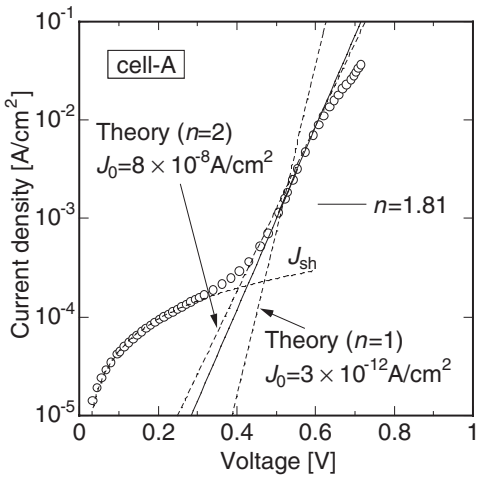

Fig. 1. Forward J–V curve of cell-A in semi-log scale.

Table II. Electrical properties derived using simple diode model for cells-A, -B, and -C. R_ss are apparent values.

	J_0 (A/cm^2)	n	R_s (Ω·cm^2)	R_{sh} (Ω·cm^2)
Cell-A	2.3×10^{-8}	1.81	2.22	2190
Cell-B	1.7×10^{-7}	2.07	4.46	1070
Cell-C	5.9×10^{-8}	1.86	3.89	1370

applied voltage was ≈ 0.7 V, and R_s derived from the slope tends to be overestimated, because the voltage drop across the diode cannot be neglected compared with that in the true series resistance at voltages close to the built-in voltage. Thus, the series resistance R_s derived from the slope is named "apparent R_s" hereafter. R_{sh} (Ω·cm^2) was taken from the slope at a voltage of -1 V in the reverse direction. In cell-B, a large n over 2 was obtained, which is different from that of an ideal diode ($n = 1$ or 2).

The obtained J_0 cannot be used to precisely derive V_{OC}, because these J_0s contain generation-recombination current. Here, V_{OC} is obtained by

$$V_{OC} = \frac{kT}{q} \ln\left(\frac{J_{SC}}{J_0} + 1\right). \quad (1)$$

For example, in cell-A, V_{OC} derived from the simple diode model using eq. (1) with $J_0 = 2.3 \times 10^{-8}$ A/cm^2 given in Table II is 0.366 V, which is far from the measured value ($V_{OC} = 0.602$ V). Therefore, this simple diode model is inadequate to analyze the electrical properties of Mx-Si solar cells, and a new equivalent circuit which can extract J_0 without generation-recombination current must be used.

2.2 *Two-diode model considering grain boundaries*

Under the assumption that the trap energy level (E_t) is equal to the intrinsic Fermi level (E_i) and that the capture cross section of electrons equals that of holes ($\sigma_n = \sigma_p = \sigma$), the forward current density (J_F) in an n^+–p diode ($V \gg kT/q$) is given by[9]

$$J_F \approx q\sqrt{\frac{D_n}{\tau_n}}\frac{n_i^2}{N_A}\exp\left(\frac{qV}{kT}\right) + \frac{qWn_i}{2}\sigma v_{th}N_t \exp\left(\frac{qV}{2kT}\right). \quad (2)$$

In eq. (2), the first and second terms are the diffusion current density and the recombination current density, respectively. Here, D_n is the diffusion constant of electrons, τ_n the minority-carrier lifetime, n_i the intrinsic carrier concentration, N_A the acceptor concentration, W the depletion-layer width, v_{th} the thermal velocity, and N_t the trap concentration.

Principally, τ_n can be calculated from the first term of eq. (2) using the forward J–V curve, but it is difficult to obtain τ_n from the data shown in Fig. 1, because the n value is considerably large as given in Table II probably due to the effect of the second term. An analysis, which can precisely separate the two current components precisely, must be employed.

An effective method is dividing a solar cell into different areas and applying ideal diode components individually to these areas. This proposal is based on the following experimental results previously reported by the authors.[7] Using a secondary ion mass spectrometry (SIMS) analysis, segregation of a typical lifetime killer, iron (Fe), was clearly found near grain boundaries, and Fe segregation areas about 100 μm wide were observed. It is well known that lifetime killers, as well as dangling bonds in grain boundaries, form deep traps for carrier recombination,[10] and their concentration affects the second term of eq. (2).

Two areas are defined, which are crystalline areas and grain boundary areas. The grain boundary areas are the areas in which lifetime killers are segregated near grain boundaries. The crystalline areas include all areas except the grain boundary areas. The crystalline areas and the grain boundary areas can be regarded as pairs of two ideal diodes of $n = 1$ and 2, which are included in eq. (2).

Figure 2 shows an example of the equivalent circuit, which includes two ideal diodes of $n = 1$ and 2 in both the crystalline areas and the grain boundary areas. In Fig. 2, subscripts C and G stand for the crystalline areas and grain boundary areas, respectively, and subscripts of 1 and 2 represent diffusion current and recombination current, respectively. r_G is the area ratio of the grain boundary areas to the total area of the cell.

This equivalent circuit, however, has a fatal drawback. J_{C1} and J_{G1} cannot be mutually separated, because it is difficult to derive r_G by whole-area optical observation of a cell. And J_{C2} and J_{G2} cannot be mutually separated for a similar reason. Therefore, extraction of each current is difficult as it is.

The equivalent circuit shown in Fig. 2 is a primitive one,

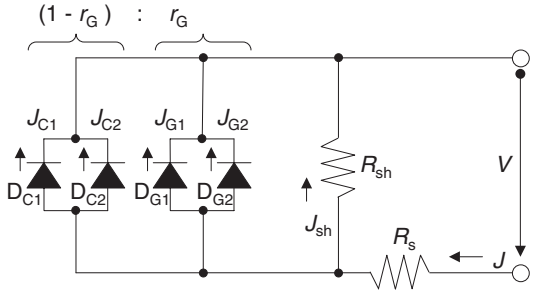

Fig. 2. Example of equivalent circuit which includes two ideal diodes of $n = 1$ and 2 in both crystalline areas and grain boundary areas.

because it is merely derived from experimental results. This circuit, however, allows further improvement to carry out analysis of Mx-Si solar cells.

2.3 DCA–RCA parallel structure for two-diode model

In order to separate diffusion current and recombination current, a "DCA–RCA parallel structure" is proposed in this study, where DCA is a "diffusion-current dominant area", which has an ideal diode of $n = 1$, and RCA is a "recombination-current dominant area", which has an ideal diode of $n = 2$. To simplify the equivalent circuit of Fig. 2, the recombination currents in the crystalline areas are merged into a current in the grain boundary areas, and the diffusion currents in the grain boundary areas are merged into a current in the crystalline areas alike.

The following explanation describes how we merge diffusion currents which flow in different areas with respect to each other. A similar explanation is applied to merging recombination currents in different areas.

Figure 3 shows the "DCA–RCA parallel structure". Mx-Si solar cells have two real areas, crystalline areas and grain boundary areas, as shown in Fig. 3(a).

Four currents can be described as shown in Fig. 3(b) using eq. (3):

$$I_F = (I_{C1} + I_{C2}) + (I_{G1} + I_{G2}), \tag{3}$$

where I_{C1} and I_{C2} are the diffusion current and the recombination current in the crystalline areas, respectively, and I_{G1} and I_{G2} are those in the grain boundary areas, respectively. The I_F is virtually separated into two kinds of current, diffusion current $(I_{C1} + I_{G1})$ and recombination current $(I_{C2} + I_{G2})$ as shown in Fig. 3(c).

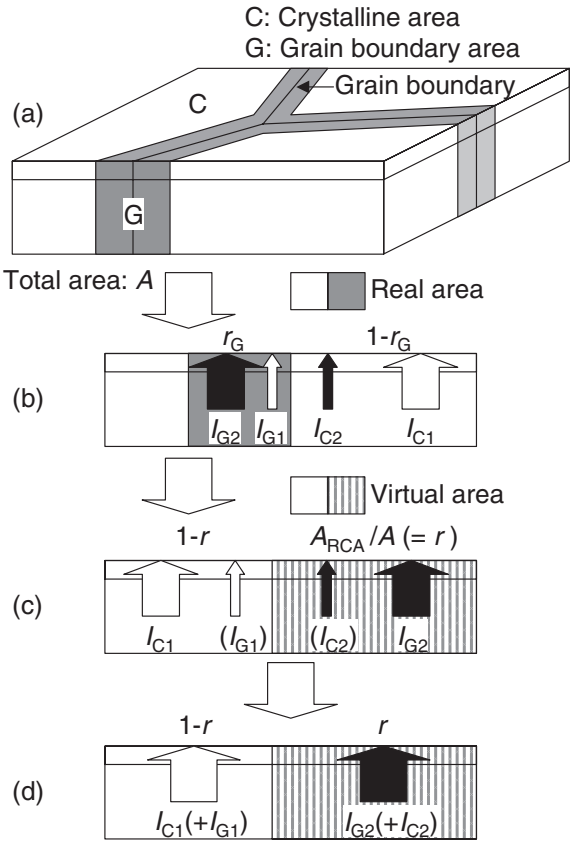

Fig. 3. DCA–RCA parallel structure. (a) Crystalline areas and grain boundary areas in Mx-Si solar cell, (b) current flows in real areas, (c) current flows in virtual areas, and (d) merging of currents in each area.

By substituting r in the virtual area for r_G in the real area, the number of parameters in the calculation can be decreased. Here, r is the area ratio of RCA to the total area (A_{RCA}/A). By increasing r, I_{C2} and I_{G1} are neglected, except in the case of a small r corresponding to a small r_G in the real area. Note that r in the virtual area differs from r_G in the real area.

In Fig. 3(d), I_{C1} and I_{G1} are merged, where I_{C1} represents diffusion current in DCA taking account of $I_{C1} \gg I_{G1}$. I_{G2} and I_{C2} are merged likewise, where I_{G2} represents recombination current in RCA taking account of $I_{G2} \gg I_{C2}$. I_{C1}/A and I_{G2}/A are transformed to current densities J_{C1} and J_{G2}, respectively.

Here, two important current densities for the subsequent analysis are defined, which are used as current components in §3. J_1 is in DCA and J_2 in RCA are described as follows:

$$J_1 \approx (1 - r)J_{C1} \equiv (1 - r) \cdot J_{01} \exp\left(\frac{qV}{kT}\right), \tag{4}$$

$$J_2 \approx r \cdot J_{G2} \equiv r \cdot J_{02} \exp\left(\frac{qV}{2kT}\right), \tag{5}$$

respectively. Here, J_{01} and J_{02} based on the first and second terms in eq. (2), are given in the following expressions, respectively.

$$J_{01} = q\sqrt{\frac{D_n}{\tau_n}}\frac{n_i^2}{N_A} \tag{6}$$

$$J_{02} = \frac{qWn_i}{2}\sigma v_{th}N_t \tag{7}$$

N_t in the DCA of the virtual area is probably much smaller than that in the RCA, because typical lifetime killer Fe is clearly found near grain boundaries.[7] The N_t in crystalline areas needs not be mentioned in distinction from that in grain boundary areas, because the recombination current in the crystalline areas is negligibly small compared with that in the grain boundary areas as discussed previously.

r may change with changes in the ideality factor n of the J–V curve, because r is defined as the area ratio of RCA to the total area A: when n becomes large, r becomes large. Normally at low voltages, $n = 2$ caused by recombination current may appear in the J–V curve. However, as shown in Fig. 1, more J_{sh} than J_0 flows at low voltages below 0.3 V. The current component of $n = 2$ is hidden by J_{sh}, and then the change of r does not appear. At high voltages above 0.6 V, $n = 2$ caused by high injection may appear. However, the diode current is restricted by R_s as in Fig. 1, and the current component of $n = 2$ is also hidden. Therefore, the change of r does not appear.

Thus, the proposed two-diode model with a fixed r for all voltages can be applied to characterization of Mx-Si solar cells, because the current of $n = 2$ does not appear as mentioned above owing to additional circuit elements such as R_{sh} and R_s.

3. Fitting Procedures for J–V Curve

3.1 Application of simple two-diode model for Mx-Si solar cells

Figure 4 shows a simple two-diode model without photocurrent applied for Mx-Si solar cells at the preliminary stage,

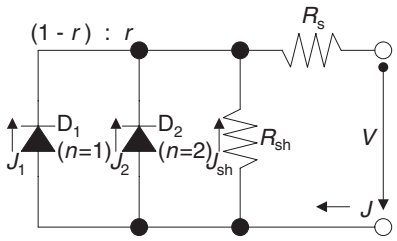

Fig. 4. Simple two-diode model for Mx-Si solar cells.

which is based on a proposed model[11] to explain the n value between 1 and 2. Diodes D_1 with $n = 1$ and D_2 with $n = 2$ are connected in parallel. D_1 and D_2 occupy the Mx-Si solar cell with the area ratio of $(1 - r)$ and r, respectively. In this model, the effects of grain boundaries are mainly expressed by D_2. For the equivalent circuit shown in Fig. 4, the total current density J is obtained from the equations given below:

$$J = J_1 + J_2 + J_{sh}, \tag{8}$$

$$J_{sh} = V_{D1}/R_{sh}, \tag{9}$$

$$V_{D1} = V_{D2} = V - (J_1 + J_2 + J_{sh})R_{sh}, \tag{10}$$

where V_{D1} and V_{D2} are the voltages applied to D_1 and D_2, and J_1, J_2, and J_{sh} are the current densities through D_1, D_2, and R_{sh}, respectively.

In order to seek the electrical properties, a *successive approximation method* was carried out using a computer. The variable parameters in each J–V curve fitting are J_{01}, J_{02}, r, and R_s. R_{sh} was determined from Fig. 1 in the reverse direction, and was treated as a fixed parameter.

In eqs. (4) and (5), the diode current density $(J_1 + J_2)$ is determined by J_{01}, J_{02}, and r. However, a solution set (J_{01}, J_{02}, r), which determines $(1 - r)J_{01}$ and rJ_{02}, does not have a unique solution set, when J_{01}, J_{02} and r take arbitrary values. In order to avoid this problem, the initial value of J_{01} was limited between $(2–3) \times 10^{-12}$ A/cm^2, because the derived V_{OC} from eq. (1) using this current level is a reasonable value for the measured V_{OC}. Other initial values of variable parameters were as follows: J_{02} is arbitrary, $r = 0.5$, and R_s = apparent R_s.

In this fitting, solution sets were determined to make the absolute value ($|\rho|$) minimum, where $|\rho|$ is the scale of correspondence between the measured points and a fitting curve. $|\rho|$ is related to the correlation coefficient. In this report, it is defined as

$$|\rho| = \frac{\sum_{i=1}^{m}(J_i - \hat{J}_{V=V_i})^2}{m}, \tag{11}$$

where m is the number of measured points and $\hat{J}$ is the fitting curve of current density.

Although fitting was carried out using this simple two-diode model, an adequate fitting curve could not be obtained. In the condition that $|\rho|$ is minimized in the total region (0–0.75 V: Approach-1), deviation of the fitting curve from the measured points occurred in the linearly increasing region (0.6–0.75 V). In contrast, in the condition that $|\rho|$ is minimized in the linearly increasing region (Approach-2), deviation of the fitting curve occurred in the J_2-dominant region, ≈0.55 V. What is worse, the obtained fitting parameters (J_{01}, J_{02}, r) given in these fittings were different for each approach as shown in Table III. Therefore, the simple two-diode model is insufficient to describe the electrical properties of Mx-Si solar cells.

Table III. Electrical properties of cell-A obtained using simple two-diode model by different fitting approaches. Approach-1: $|\rho|$ optimized in total region (0–0.75 V); Approach-2: $|\rho|$ optimized in linearly increasing region (0.6–0.75 V).

	J_{01} (A/cm^2)	J_{02} (A/cm^2)	r	R_s (Ω·cm^2)	R_{sh} (fixed) (Ω·cm^2)
Approach-1	2.8×10^{-12}	7.8×10^{-8}	0.67	2.9	2190
Approach-2	2.1×10^{-12}	6.8×10^{-7}	0.94	1.5	2190

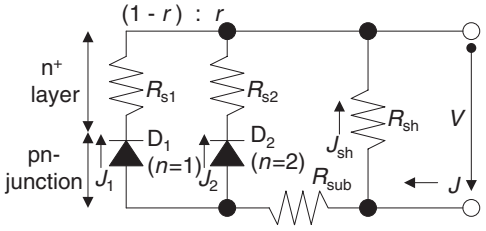

Fig. 5. Nonequivalent-R_s-connected two-diode model for Mx-Si solar cells.

3.2 *Proposal of Nonequivalent-R_s-connected two-diode model for Mx-Si solar cells*

Considering the segregation of impurities near grain boundaries, microscopic inhomogeneity in the resistivity of DCA and RCA must be expressed in the equivalent circuit. Figure 5 shows a nonequivalent-R_s-connected two-diode model proposed in this report. In solar cells with a shallow junction, majority carriers in the n^+ layer flow parallel to the pn junction at most by half the distance between individual finger electrodes, and are easily affected by the heterogeneity in resistivity. In this model, series resistances R_{s1} and R_{s2} were attached to diodes D_1 and D_2, respectively. In Mx-Si solar cells with 1 Ω·cm resistivity and 300 μm thickness, the specific resistance of the p-type substrate (R_{sub}) can be estimated as about 0.03 Ω·cm^2, which is added in order to separate R_{s1} and R_{s2} from R_{sub} in this model.

In the fitting using this nonequivalent-R_s-connected two-diode model, two more variable parameters, R_{s2}/R_{s1} and R_{s1}, were used. R_{sub} was treated as a fixed parameter. The initial values of variable parameters were given as follows: J_{01} and J_{02} are arbitrary, $r = 0.5$, $R_{s2}/R_{s1} = 1$, and R_{s1} = apparent R_s.

Figures 6(a) and 6(b) show the fitting result for the forward J–V curve of cell-A. To verify the curve fitting, the semi-log scale and linear scale are shown. In Fig. 6(a), the fitting curve properly expresses the measured values precisely. Particularly, the accuracy of fitting at voltages higher than 0.5 V was improved. Figure 6(b) also shows the accuracy of fitting in the linearly increasing region. It should be noticed that the obtained five fitting parameters $(J_{01}, J_{02}, r, R_{s1}, R_{s2})$ given in Figs. 6(a) and 6(b) are exactly the same. The electrical properties thus obtained for cells-A, -B, and -C are listed in Table IV.

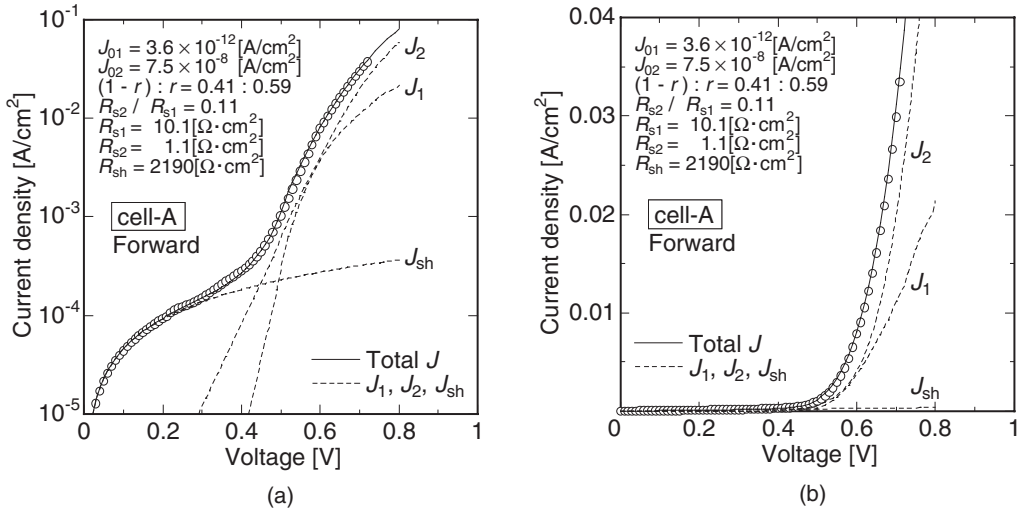

Fig. 6. Fitting result of forward J–V curve for cell-A by nonequivalent-R_s-connected two-diode model, (a) in semi-log scale, and (b) in linear scale.

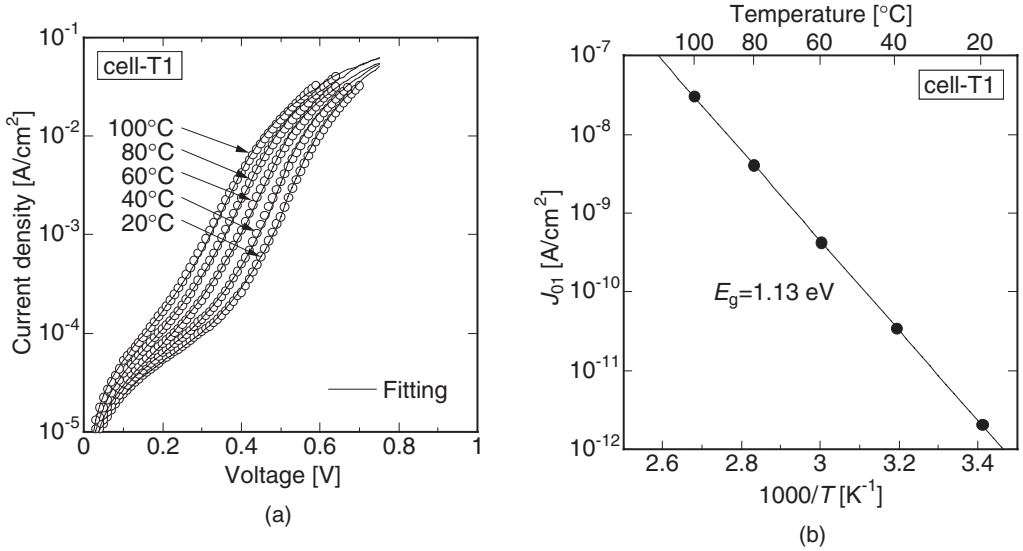

Fig. 7. (a) Fitting result of forward J–V curves for cell-T1 by nonequivalent-R_s-connected two-diode model in semi-log scale. Temperature was changed from 20 to 100°C in steps of 20°C. (b) Temperature dependence of J_{01} and derivation of E_g.

Table IV. Electrical properties of cells-A, -B, -C, -T1, and -T2 at room temperature obtained using nonequivalent-R_s-connected two-diode model.

	η (%)	J_{01} (A/cm^2)	J_{02} (A/cm^2)	r	R_{s2}/R_{s1}	R_{s1} (Ω·cm^2)	R_{s2} (Ω·cm^2)	R_{sh} (fixed) (Ω·cm^2)
Cell-A	14.4	3.6×10^{-12}	7.5×10^{-8}	0.59	0.11	10.1	1.1	2190
Cell-B	12.6	6.3×10^{-12}	1.4×10^{-7}	0.67	0.34	10.3	3.5	1070
Cell-C	11.0	1.2×10^{-11}	1.3×10^{-7}	0.74	0.50	7.7	3.9	1370
Cell-T1	8.6	2.0×10^{-12}	2.4×10^{-7}	0.35	6.14	3.6	22.1	4400
Cell-T2	10.1	2.8×10^{-12}	1.2×10^{-7}	0.59	9.82	3.9	38.3	17000

Analysis of the temperature characteristic is necessary, because temperature is an important parameter which governs semiconductor carrier transport. For cells-T1 and -T2, the curve fitting was carried out by a successive approximation method using the nonequivalent-R_s-connected two-diode model, in which the parameters of J_{01}, J_{02}, r, R_{s1}, and R_{s2} were regarded as variable parameters described above. Temperature was changed from 20 to 100°C in steps of 20°C.

Figure 7(a) shows the fitting result of forward J–V curves for cell-T1 in the semi-log scale. The curve fitting was successfully carried out at each temperature without adding

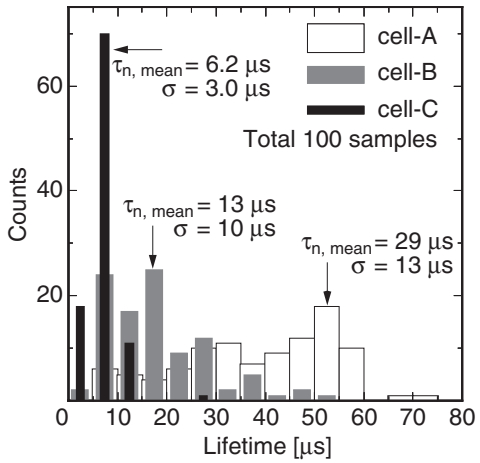

Fig. 8. Histograms of τ_ns obtained by reverse recovery switching analysis[7] for 100 samples of cells-A, -B, and -C.

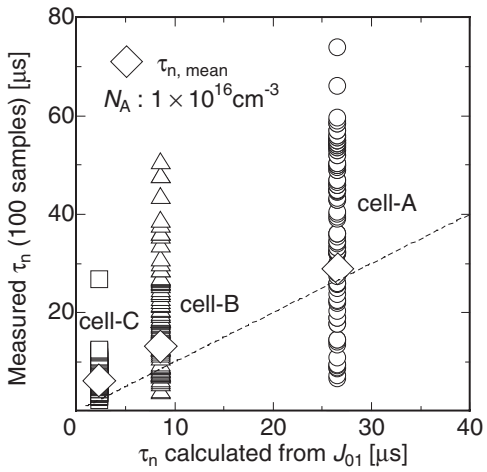

Fig. 9. Correlation between τ_n calculated from J_{01} and harmonic mean values of measured τ_n given from Fig. 8.

other parameters. The electrical parameters obtained for cells-T1 and -T2 at room temperature (20°C) are listed in Table IV together with those of cells-A, -B and -C. Figure 7(b) shows the temperature dependence of J_{01} for cell-T1, which gives the following relation.

$$J_{01} \sim \exp\left(-\frac{\Delta E}{kT}\right) \tag{12}$$

The activation energy, ΔE, obtained from the slope of the curve is 1.13 eV, which is close to the energy band gap E_g of Si from a reference.[12] Since J_{01} represents the diffusion current, which is proportional to the square of intrinsic carrier concentration determined by the energy band gap, this result indicates that J_{01} is successfully extracted using the nonequivalent-R_s-connected two-diode model.

4. Validity of Fitting Parameters

The electrical properties of solar cells were determined precisely using the fitting parameters of the successive approximation method. To verify the validity of the fitting parameters, some electrical properties, τ_n, r, V_{OC}, and R_{sh}, were compared with those obtained by other methods.

4.1 Minority-carrier lifetime τ_n

Using the value of J_{01} in Table IV, τ_n can be calculated from eq. (6). By capacitance–voltage (C–V) measurement of locally divided cells with $3 \times 3\,mm^2$ size, N_A was obtained as about $(0.5–1) \times 10^{16}\,cm^{-3}$. Thus, in the calculation, N_A was assumed as $1 \times 10^{16}\,cm^{-3}$. D_n was also assumed as about $30\,cm^2/s$.[13] Figure 8 shows the histograms of τ_ns for 100 samples ($12 \times 12\,mm^2$, 10×10) locally divided from cells-A, -B, and -C ($125 \times 125\,mm^2$ in size). τ_ns were obtained by reverse recovery switching transient analysis.[7] Figure 9 shows the correlation between the values of τ_ns calculated from J_{01} and those obtained by the reverse recovery switching transient analysis shown in Fig. 8. The broken line shows $\tau_{n(\text{from } J_{01})} = \tau_{mean}$, where τ_{mean} is the harmonic mean value of τ_ns for the 100 samples of each cell. The τ_n estimated from J_{01} well corresponds to the measured τ_{mean}. The result suggests that τ_n, which determines the magnitude of J_{SC}, can be estimated successfully using J_{01} extracted from the J–V curve measured in the dark condition.

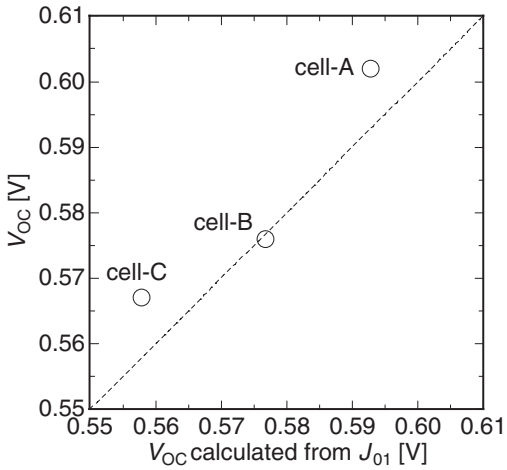

Fig. 10. Correlation between V_{OC} calculated from J_{01} and measured V_{OC} in Table I.

4.2 Area ratio of RCA r

r is defined as the area ratio of RCA to the total area in the cell. In Mx-Si solar cells, about 100-μm-wide band-shaped Fe segregation areas were observed.[7] Under the assumption that the width of the band is about 100 μm at all grain boundaries, the ratio of grain boundary areas to the total area was estimated. From the 100 samples of cell-A, a sample with a τ_n of 29 μs (harmonic mean value for cell-A) was picked up, and its total length of grain boundaries was measured using a Nomarski microscope.

The grain boundary occupation ratio r_G in the real area of the sample was ≈ 0.11. In contrast, the r extracted from the J–V curve of cell-A was 0.59 as shown in Table IV. The possible reason why r is much larger than r_G is the considerable recombination current in the crystalline area due to metal spiking effects during formation of electrodes through passivation coating by a fire-through process.

4.3 Open-circuit voltage V_{OC}

V_{OC} is derived by eq. (1) using the obtained J_{01} in Table IV instead of J_0 in Table II. Figure 10 shows the correlation between the V_{OC} calculated from J_{01} and the

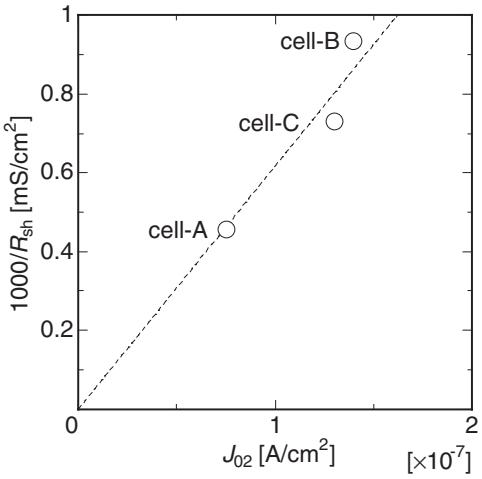

Fig. 11. Correlation between $1/R_{sh}$ and J_{02}.

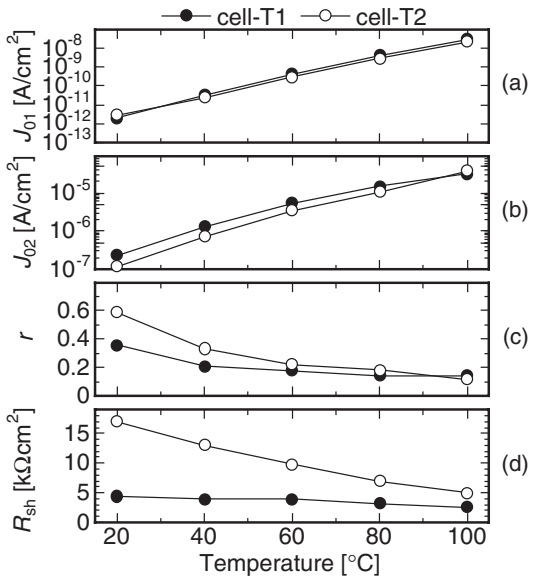

Fig. 12. Temperature dependence of (a) J_{01}, (b) J_{02}, (c) r, and (d) R_{sh} for cells-T1 and -T2.

measured V_{OC} given in Table I. The broken line shows $V_{OC(\text{from } J_{01})} = V_{OC}$. This result also suggests that J_{01} is recognized as valid.

Since J_{01} is strongly related to J_{SC} and V_{OC}, J_{01} can be regarded as the "power factor", which indicates the intrinsic output performance of solar cells without various kinds of losses.

4.4 *Effects of J_{02} on cell performance*

Figure 11 shows the correlation between $1/R_{sh}$ and J_{02}, from which the proportional relation between $1/R_{sh}$ and J_{02} is found. To explain this result, the origin of J_{02} was examined. J_{02} is given by eq. (7) and its value is calculated from the J–V curve of each solar cell. As described in §2, R_{sh} was taken from the slope at a voltage of -1 V. The width of the depletion layer (W), in eq. (7), for a one-sided abrupt junction is given by

$$W = \sqrt{\frac{2\epsilon_s(V_{bi} - V)}{qN_A}}. \tag{13}$$

In eq. (13), ϵ_s is the dielectric constant of the semiconductor, and V_{bi} is the built-in voltage. The value of W is thought to be constant, because the variables, V and N_A, in eq. (13) are approximately the same for cells-A, -B, and -C. Thus, in eq. (7), q, W, n_i, and v_{th} are constant, and σ is probably constant, because Fe, the origin of the trap, mainly affects the τ_ns in those solar cells. Therefore, the difference in J_{02} is caused by the difference in trap concentration N_t.

The reverse current density J_R is given by

$$J_R \approx J_{01} + J_{02} \approx \frac{qWn_i}{2}\sigma v_{th}N_t, \tag{14}$$

because $J_{01} \ll J_{02}$ in any case. Thus, $1/R_{sh}$ is proportional to J_{02}, which depends on only N_t.

Moreover, J_{02} evidently causes a decrease in FF. FF is degraded by both an increase in n and a decrease in R_{sh}. After all, J_{02} can be regarded as the "loss factor", which indicates intrinsic output loss. Cell-A has a large power factor and a small loss factor indicating a higher η. Cell-B decreases its η by a rather large loss factor even though it has a considerably large power factor, and has a margin to improve its performance. In contrast, cell-C has a small power factor with a rather large loss factor indicating a lower η.

4.5 *Temperature dependences of other parameters*

Figure 12 shows temperature dependences of (a) J_{01}, (b) J_{02}, (c) r, and (d) R_{sh} for cells-T1 and -T2. From Fig. 12(a), τ_ns of crystalline areas are considered to be almost the same between cells-T1 and -T2 because of similar J_{01} values. From Figs. 12(b) and 12(d), however, cell-T2 is better than cell-T1 in the loss factor, J_{02} and R_{sh}. The difference is probably caused by metallization of electrodes. Metal spiking through passivation coating by a fire-through process increases the number of defects and impurities under electrodes, which increase J_{02} and decrease R_{s2} and R_{sh}. From Table IV, cells-T1 and -T2 must be exposed to a lower-temperature or shorter-time fire-through process than that used for cells-A, -B, and -C, because the former has larger R_{s2} and R_{sh} values than the latter. Actually, cells-T1 and -T2 are from different batches of cells-A, -B, and -C.

Here, the temperature dependences of r and R_{sh} are discussed. In Fig. 12(c), r has a temperature dependence at low temperatures, although the dependence is hardly found at high temperatures. Generally, J_1/J_2, the ratio of diffusion current/recombination current, in a pn diode tends to be larger as temperature becomes higher, which makes r smaller. The rs of cells-T1 and -T2 asymptotically approach 0.1 at a high temperature. The asymptotic value can be regarded as the ratio of r_G in the real area.

In Fig. 12(d), R_{sh} of cell-T2 has a strong temperature dependence, although that of cell-T1 has a weak one. The temperature dependence of cell-T2 can be explained by assuming an additional shunt which is composed of a diode and a resistance in series, because the current passing through the resistance in series depends on the temperature by the diode.

5. Conclusions

In order to extract electrical properties precisely, I–V

measurement in the dark condition was carried out for Mx-Si solar cells. A nonequivalent-R_s-connected two-diode model including a diffusion-current dominant area (DCA) and a recombination-current dominant area (RCA) was proposed as a new equivalent circuit, and a successive approximation method was applied for seeking fitting parameters precisely using this model. Fitting parameters were successfully extracted, and the verification of these parameters was carried out on the basis of τ_n measurement and temperature characteristics.

By using the parameters J_{01} as a power factor and J_{02} as a loss factor, solar cells can be compared with each other, and the way to improve solar cell performance may be easily found.

1) R. Shimokawa and Y. Hayashi: J. Appl. Phys. **59** (1986) 2571.
2) M. David, H. Matsunami and T. Fuyuki: Sol. Energy Mater. Sol. Cells **65** (2001) 445.
3) S. K. Datta, K. Mukhopadhyay, S. Bandopadhyay and H. Saha: Solid-State Electron. **35** (1992) 1667.
4) K. Chakrabarty and S. N. Singh: Solid-State Electron. **39** (1996) 577.
5) Z. Ouennoughi and M. Chegaar: Solid-State Electron. **43** (1999) 1985.
6) M. Chagaar, Z. Onennoughi and A. Hoffmann: Solid-State Electron. **45** (2001) 293.
7) K. Kurobe, M. Miura, K. Hirano and H. Matsunami: Sol. Energy Mater. Sol. Cells **74** (2002) 183.
8) K. Nishioka, N. Sakitani, K. Kurobe, Y. Yamamoto, Y. Ishikawa, Y. Uraoka and T. Fuyuki: Jpn. J. Appl. Phys. **42** (2003) 7175.
9) S. M. Sze: *Physics of Semiconductor Devices* (John Wiley & Sons, New York, 1981) 2nd ed.
10) Y. Hayamizu, T. Hamaguchi, S. Ushio, T. Abe and F. Shimura: J. Appl. Phys. **69** (1991) 3077.
11) J. Zhao, A. Wang, P. P. Altermatt and M. A. Green: Proc. 26th IEEE Photovoltaic Specialists Conf., Anaheim, 1997, p. 227.
12) C. D. Thurmond: J. Electrochem. Soc. **122** (1975) 1133.
13) H. J. Hovel: *Semiconductors and Semimetals* (Academic Press, New York, 1975) Vol. 11, Solar Cells.